

Article

Two New Benthic Diatoms of the Genus *Achnantheidium* (Bacillariophyceae) from the Hangang River, Korea

Minzi Miao ^{1,†}, Zhun Li ^{2,†} , Eun-A Hwang ¹, Ha-Kyung Kim ¹, Hyuk Lee ³
and Baik-Ho Kim ^{1,4,*} 

¹ Department of Environmental Science, Hanyang University, Seoul 04763, Korea; miaominzi@naver.com (M.M.); euna1602@naver.com (E.-A.H.); hosang9022@naver.com (H.-K.K.)

² Biological Resource Center/Korean Collection for Type Cultures (KCTC), Korea Research Institute of Bioscience and Biotechnology, Jeongseup 56212, Korea; lizhun@kribb.re.kr

³ National Institute of Environmental Research, Incheon 22689, Korea; ehyuk72@korea.kr

⁴ Department of Life Science and Research Institute for Natural Sciences, Hanyang University, Seoul 04763, Korea

* Correspondence: tigerk@hanyang.ac.kr; Tel.: +82-2-2220-0960

† These authors contributed equally as co-first authors.

<https://www.ipni.org/urn:lsid:ipni.org:authors:20045093-1>

Received: 25 June 2020; Accepted: 20 July 2020; Published: 21 July 2020



Abstract: Two new benthic freshwater species belonging to the genus *Achnantheidium* were found in Korea. *Achnantheidium ovale* sp. nov. and *A. cavitatum* sp. nov. are described as new species based on light and scanning electron microscopy observations and molecular analyses. Both species are compared with the type material of morphologically similar taxa. *Achnantheidium ovale* differs from other species belonging to the *A. pyrenaicum* complex in outline, striation pattern, raphe central endings, and freestanding areolae at the apices. *Achnantheidium cavitatum* differs from other species in the *A. minutissimum* complex in outline, broad axial central area in the raphe valve, and slit-like areolae near the axial central area. We assessed their molecular characteristics by analyzing nuclear small subunit (SSU) rRNA and chloroplast-encoded *rbcl* gene sequences. Both the morphological comparison and the SSU and *rbcl* sequence analyses provide strong evidence to support the recognition of *A. ovale* and *A. cavitatum* as new species.

Keywords: *Achnantheidium*; freshwater; molecular phylogeny; morphology; *rbcl*; SSU; taxonomy

1. Introduction

The genus *Achnantheidium* Kütz. has been considered a subgenus of *Achnanthes* Bory [1]. Round et al. [2] restituted the genus rank to *Achnantheidium* and distinguished *Achnanthes* from *Achnantheidium* based on the areola, raphe, girdle, and plastid characteristics. Czarnecki [3] then transferred *Achnanthes minutissima* Kütz. to *Achnantheidium* as *A. minutissimum* (Kütz.) Czarn. The genus *Achnantheidium* was then redefined by Round and Bukhtiyarova [4].

The genus *Achnantheidium* currently includes freshwater monoraphid species with the following characteristics: (1) linear-lanceolate to lanceolate elliptic cells with length and width less than 30 µm and 5 µm, respectively, (2) concave raphe valve, uniseriate striae, and a wide central area; (3) a well-developed raphe that can be straight or turned to one side [4]. Because of their small size and inadequate morphological features, *Achnantheidium* species can be complicated to identify. Currently, species in the genus *Achnantheidium* can be divided into three major groups: (1) the *A. minutissimum* complex, which includes species with straight raphe fissures on the apical area;

(2) the *A. pyrenaicum* complex, with species with hooked terminal raphe fissures; (3) the *A. exiguum* complex, with species that have terminal raphe endings deflecting to opposite sides [5–7].

Some new *Achnanthyidium* species have been recently reported: *A. sieminskae* [8], *A. barbei* [9], and *A. costei* [9] in the *A. minutissimum* complex; *A. rivulare* by Potapova and Ponader [10], *A. hoffmannii* [11], and *A. delmontii* [12] in the *A. pyrenaicum* complex; *A. initium* [13] in the *A. exiguum* complex.

Species of the genus *Achnanthyidium* have been reported to live in a wide variety of ecological conditions, from oligotrophic to eutrophic and from alkaline to acidic environments [14]. Species of *Achnanthyidium* respond differently to water chemistry conditions. Therefore, species-level identification can produce more accurate bioassessments [15]. Because *Achnanthyidium* species are both common and abundant, it is very important to identify the ecological environment of each species and propose an adequate classification of all the *Achnanthyidium* species [16].

Diatom valves are perforated by areolae (pores) that allow communication between the diatom's protoplast and the surrounding environment [17]. The development of internal hymenes (cf. Cox [18]) is the final stage in valve morphogenesis [19]. Areolae have two types of ultrastructure: poroid areolae are not markedly constricted on one surface of the valve, whereas loculate areolae are markedly constricted on one surface and occluded on the other [19]. Ross et al. [20] defined loculate areolae as a regular perforation through the basal siliceous valve, usually occluded by a velum (cribrum, rota, vola) or a rica. Mann [21] refined the definition of pore occlusion as a delicate siliceous membrane that crosses the entire pore, called a hymen (=rica of Ross et al. [20]). Cox [22] considered some structural characteristics of diatoms are highly consistent with raphid taxa—e.g., raphe construction, type of pore occlusion (hymenes, cribrum, etc.)—Whereas other characteristics, such as pore shape, degree of surface silicification, and raphe fissure path, could be more susceptible to variation. Yana and Mayama [23] proposed that, from the internal view, the areolae of *Achnanthyidium pseudoconspicuum* var. *yomensis* Yana & Mayama [23] are loculate with incomplete vimines. Two types of areolae were detected on the valve face: round (various sizes in different taxa) and slit-like, which always appeared close to the valve margin in *A. catenatum*, *A. dolomiticum*, and *A. saprophilum* [24].

Sequences of a variety of genes such as ITS, COI, large subunit rRNA, small subunit rRNA (SSU), and ribulose-1, 5-bisphosphate carboxylase/oxygenase (*rbcL*), are currently being used to propose phylogenetic relationships among diatoms [25]. Of them, previous studies have shown that SSU is a powerful tool for inferring phylogenetic relationships at all taxonomic levels [26]. SSU rRNA gene sequences have been widely used to represent the major diatom lineages [27–32]. The *rbcL* gene is located in a single-copy region of the chloroplast genome [25,33]. Because it only rarely has insertions or deletions, the *rbcL* gene is considered better than the SSU gene for studies of diatom evolution from order to genus levels [34].

The sequences of some Achnanthidiaceae genera were not added to molecular phylogenetic datasets until 2016 [35]. Round et al. [2] described the family Achnanthidiaceae to include two genera, *Achnanthyidium* and *Eucoconeis* Cleve ex Meister. However, according to Kulikovskiy et al. [35], genera such as *Rossithidium* Round & Bukhtiyarova, *Psammothidium* Bukhtiyarova & Round, and *Lemnicola* Round & Basson should also be included in this family. The taxonomy of achnanthoid diatoms has mostly been based on morphological data, and molecular studies with the SSU rRNA and *rbcL* genes should also be performed [36].

As part of documenting the distribution of diatoms from oligotrophic environments in Korea, we report the morphological characteristics of two *Achnanthyidium* species and compare nuclear-encoded SSU rRNA and chloroplast-encoded *rbcL* gene sequences with those of related species. From those results, we describe two new species, *Achnanthyidium ovale* sp. nov. and *Achnanthyidium cavitatum* sp. nov. Upon addition of the two new species, 169 *Achnanthyidium* species are known globally and 22 in Korea (AlgaeBase & NIBR).

2. Materials and Methods

2.1. Sample Collection, Isolation, and Culture

To collect diatoms, two or three pebbles were collected from the littoral zones (0.1 m depth) of rivers. The sampling points at which diatoms were collected are shown in Table 1 and located in the Hangang River, Republic of Korea (Figure 1). Epilithon was collected from the surfaces of the stones using a toothbrush. Single diatom cells were isolated using a Pasteur pipette (Hilgenberg GmbH, Germany) and the capillary method [37] under an Olympus CKX41 inverted microscope (Olympus, Tokyo, Japan). Cells were isolated and cultured in 96-well cell plates, and each well contained 160 μL of Diatom Medium (DM) [38]. After 10–14 days of isolation, diatoms reached the exponential growth stage [39]. The cells that grew and had a healthy aspect were transferred into 24-well cell plates with 1 mL of DM. Again, after 10–14 days, the cells that were in good condition were transferred to 50 cm^3 culture flasks with 20 mL of DM. To maintain healthy cells, each strain was sub-cultured at 40-day intervals. All the strains were cultured at 20 $^\circ\text{C}$, with an irradiance of $c. 50 \mu\text{mol quanta m}^{-2} \text{s}^{-1}$, and a 12:12 h light: dark cycle with cool white fluorescent light. Two new diatom cultures were eventually established; of these, one culture was used for this study. The other two cultures were preserved at a lower temperature ($<10 \text{ }^\circ\text{C}$) and light intensity ($<20 \mu\text{mol m}^{-2} \text{s}^{-1}$) for growth limitation.

Table 1. Environmental variables at the sampling sites of *Achnantheidium ovale* sp. nov. and *A. cavitatum* sp. nov.

	<i>Achnantheidium ovale</i>	<i>Achnantheidium cavitatum</i>
Coordinates	37°31'59 α " N, 128°0'42" E	38°4'28" N, 127°24'52" E
pH	7.07	6.72
Dissolved oxygen	5.93	7.93
Temperature ($^\circ\text{C}$)	11.71	11.29
Velocity (cm/sec)	80	20
Conductivity ($\mu\text{S/cm}$)	57	148
Turbidity (NTU)	0.0	3.1

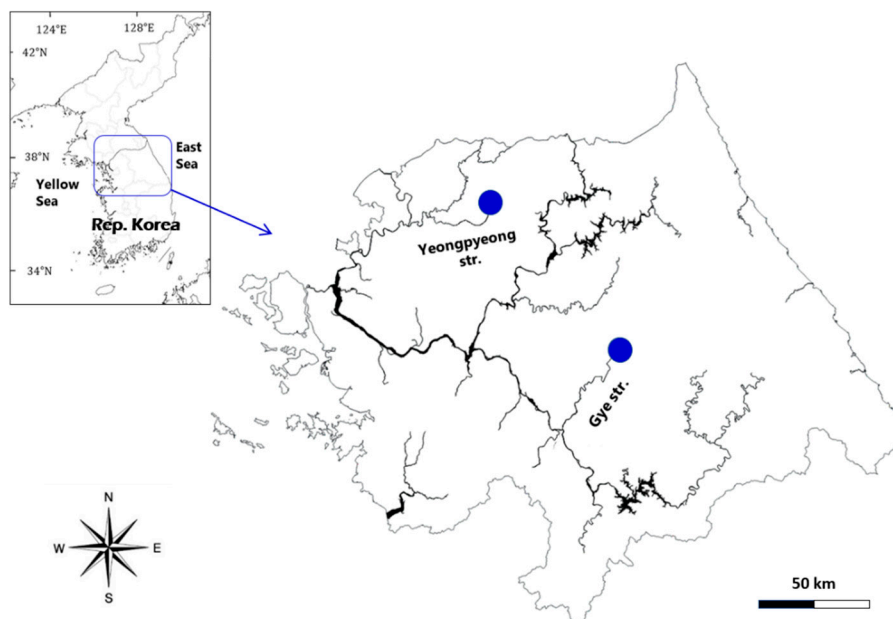


Figure 1. A map showing the sampling sites of two diatoms as *Achnantheidium ovale* from Gye Stream in Hoengseong, Kangwon-do and *A. cavitatum* from the upstream of Yeonpyeong in Pocheon city, Gyeonggi-do, the Hangang River, Republic of Korea.

2.2. Light Microscopy (LM)

For LM, both natural and cultured cells were fixed with Lugol solution. To remove organic compounds, HNO₃ and H₂SO₄ (1:3) were added to the samples, which were then boiled at 100 °C for 2–3 min. To remove the acid from the oxidized cultures, the samples were washed four times with distilled water, following one day of sedimentation. Morphological characteristics were observed using an upright microscope (Nikon E600, Nikon, Tokyo, Japan). Slides of the washed frustules were mounted using Wako Mountmedia (Wako Pure Chemical Industries, Ltd., Osaka, Japan). Light micrographs were collected at 1000× magnification using an MSC-C5.0 microscope digital camera (SONY, Tokyo, Japan). Measurements of length and width of frustules were obtained from at least 50 diatom cells.

2.3. Scanning Electron Microscopy (SEM)

For SEM, the washed samples were gently filtered through a 0.2-µm pore-sized GTTP Millipore filter membrane (Millipore Filter Corporation, Cork, Ireland) using gravity. The membrane was then stuck to the SEM stubs with carbon tape (Shintron Enterprise CO., Ltd., Kaohsiung, Taiwan). Mounted specimens were dried for at least 12 h at room temperature. Finally, the specimens were coated for 120 s with platinum and examined using field emission SEM (Nova Nano SEM 450, FEI Inc., Hillsboro, OR, USA).

2.4. DNA Extraction, PCR Amplification, and Sequencing

Clonal cultures (10 mL) were prepared in the mid-logarithmic growth phase and centrifuged in a conical tube at 4000× *g* for 10 min. A DNeasy Plant Mini Kit (Qiagen, Valencia, CA, USA) was used for genomic DNA extraction. PCR reactions were performed in 40 µL reaction mixtures, and the primers used in the PCR amplification of SSU and *rbcl* genes are shown in Table 2. Each reaction mixture contained 23.8 µL of distilled water, 4 µL of 10× Ex PCR Buffer (TaKaRa, Tokyo, Japan), 4 µL of dNTP (deoxyribonucleotide triphosphate) (TaKaRa), 0.2 µL of ExTaq polymerase (TaKaRa), 2 µL of each primer, and 4 µL of DNA template. PCR amplification was carried out in a Bio-Rad iCycler (Bio-Rad, Hercules, CA, USA) using the following conditions: pre-denaturation at 94 °C for 4 min; 37 cycles at 94 °C for 20 s, 56 °C for 30 s, and 72 °C for 50 s; and a final extension at 72 °C for 5 min. The PCR products were separated by electrophoresis in 1% agarose gel with a staining solution (Genetics, Dueren, Germany) and then sent to the company BIONICS (ISO: 9001, Seoul, Korea) for SSU rRNA and *rbcl* gene sequencing.

Table 2. Primers used to amplify and sequence the SSU rRNA and *rbcl* genes.

Gene	Primer	Nucleotide Sequence (5' to 3')	Reference
SSU rRNA	AT18F01	YAC-CTG-GTT-GAT-CCT-GCC-AGT-AG	[40]
	AT18R02	GTT-TCA-GCC-TTG-CGA-CCA-TAC-TCC	[40]
	AT18F02	AGA-ACG-AAA-GTT-AAG-GGA-TCG-AAG-ACG	[40]
	AT18R01	GCT-TGA-TCC-TTC-TGC-AGG-TTC-ACC	[40]
<i>rbcl</i>	F3	GCT-TAC-CGT-GTA-GAT-CCA-GTT-CC	[25]
	R3	CCT-TCT-AAT-TTA-CCA-ACA-ACT-G	[25]

2.5. Phylogenetic Analyses

Sequences were viewed and assembled in ContigExpress (Vector NTI version 1.6, Invitrogen, Grand Island, NY, USA). The SSU rRNA and *rbcl* sequences from this study were deposited in the National Center for Biotechnology Information (NCBI) GenBank (Table 3). Multiple sequence alignment between the sequences generated in this study and those obtained from the NCBI database was performed using ClustalW [41] in MEGA version 7.0 [42]. The alignments were manually edited, and ambiguously aligned characters were excluded using MEGA version 7.0 [42]. MEGA 7.0 was also used to calculate the genetic distance (*p*-distance) by means of a bootstrap method with 1000 replicates

and a Kimura 2-parameter model [42]. The final alignment of the SSU rDNA dataset contained 39 taxa and 1628 characters (including gaps introduced for alignment), and the *rbcL* dataset contained 52 taxa and 1628 characters (1390 bp). Sequences of *Aulacoseira granulata* were used as outgroups for the SSU and *rbcL* phylogenetic trees.

Table 3. Strains of *Achnanthydium ovale* sp. nov. and *A. cavitatum* sp. nov. isolated in the Hangang River, Republic of Korea.

Species	Strain	Taxonomic Position	Gene Type	Locality	GenBank Accession No.
<i>Achnanthydium ovale</i> sp. nov.	HYU-D036	<i>Achnanthes</i> ; <i>Achnanthydiaceae</i>	SSU	Korea	MK578710, this study
<i>Achnanthydium ovale</i> sp. nov.	HYU-D036	<i>Achnanthes</i> ; <i>Achnanthydiaceae</i>	<i>rbcL</i>	Korea	MK639354, this study
<i>Achnanthydium cavitatum</i> sp. nov.	HYU-D037	<i>Achnanthes</i> ; <i>Achnanthydiaceae</i>	SSU	Korea	MK578711, this study
<i>Achnanthydium cavitatum</i> sp. nov.	HYU-D037	<i>Achnanthes</i> ; <i>Achnanthydiaceae</i>	<i>rbcL</i>	Korea	MK639355, this study

Phylogenetic trees for the sequence alignments (SSU and *rbcL*) were inferred from maximum likelihood (ML) analyses (using RaxML version 8 [43]) and Bayesian inference (using MrBayes version 3.2: [44]). The general time-reversible model with parameters accounting for γ -distributed rate variation across sites was used in all analyses, taking into account a 6-class gamma. Bootstrap analyses for both datasets were carried out for ML with 1000 replicates to evaluate statistical reliability. The Markov chain Monte Carlo method was used with four runs for 10 million generations, sampling every 100 generations. A majority-rule consensus tree was created to examine the posterior probabilities of each clade. The final trees were visualized with MEGA version 7.0.

3. Results

3.1. Species Description

3.1.1. *Achnanthydium ovale* M. Miao & B.-H. Kim, sp. nov.

Figure 2 (LM), Figure 3, and Figure 4 (SEM) here.

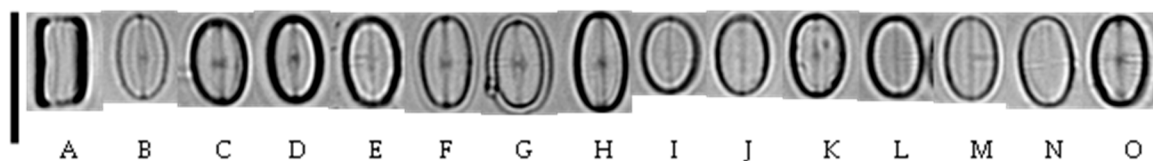


Figure 2. LM of *Achnanthydium ovale* sp. nov. taken from the holotype population (180409KCB8B40511). Scale bar = 10 μ m. (A). Girdle view of *A. ovale*. (B–H) Raphe view of cell valve. (I–O) Rapheless view of cell valve.

Description: Cells are elliptical, 6.3–7.7 μ m long, and 3.8–4.1 μ m wide. Striae density varies by location; 30–35 in 10 μ m in the center, and up to 55 near the apices of the raphe valve. The number of striae on the primary side is higher than on the secondary side of the rapheless and raphe valves. Therefore, a “T” pattern can be seen in the LM images (Figure 2B–O).

At the external part of the raphe valve, the striae are parallel but radiate very slightly and curve near the apices. The shorter striae in the central part consist of 4–6 areolae. The terminal fissures of the raphe are hooked toward the same side (arrow in Figure 3A). Central raphe endings are laterally expanded (Figure 3C). The sternum is narrow and slightly broader in the central area (Figure 3A).

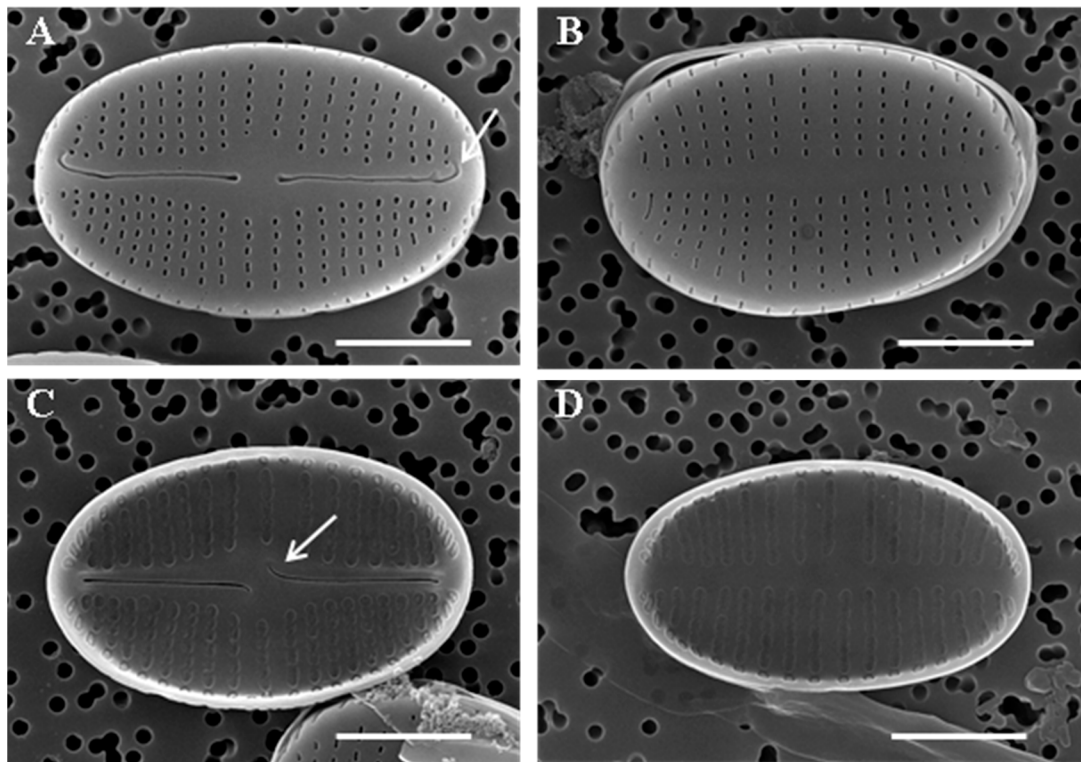


Figure 3. SEM of *Achnanthidium ovale* sp. nov. taken from the holotype population (180409KCB8B40511). Scale bar = 2 μ m. (A) External view of raphe valve. Hooked terminal raphe fissures (arrow). (B) External view of rapheless valve. (C) Internal view of raphe valve. Central raphe endings deflect in the opposite direction in internal view (arrow). (D) Internal view of rapheless valve.

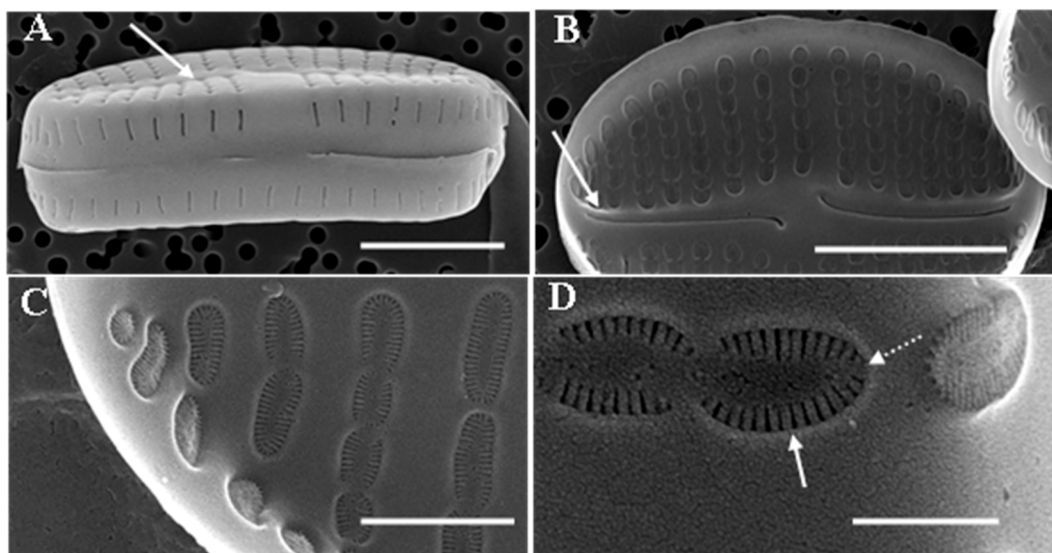


Figure 4. SEM of *Achnanthidium ovale* sp. nov. taken from the holotype population (180409KCB8B40511). (A) Convex rapheless valve with shallow V axial area (arrow). Scale bar = 2 μ m. (B) The raised helictoglossae (arrow) and unconnected vimines above the adjacent areolae in internal view. Scale bar = 2 μ m. (C) Internally, areolae structures are hymenes with marginal slits which have different thickness (arrow). Scale bar = 0.5 μ m. (D) The areolae close to the margin area separate from neighboring areolae. Hymenes with perforations of a parallel array type (solid arrow) and centric array type (dotted arrow). Scale bar = 0.2 μ m.

The rapheless valve is convex. The axial area is below the valve plane, and it forms a shallow V (arrow in Figure 4A). A row of slit-like areolae is present on the mantles of the raphe and rapheless valves (Figure 4A). In the oblique view, the helictoglossae are raised internally (Figure 4B, arrow). Areolae are occluded by hymens, which are connected in adjacent areolae. Pairs of unconnected vimines are present above the adjacent areolae (Figure 4B); however, the areolae near the margin area are separate from the neighboring areolae. The structure of the areolae from the inner parts of both valves is formed by hymenes with marginal slits; the thickness of the central disk differs from that of the marginal area (Figure 4C). Hymenes have perforations of the parallel array type (solid arrow) and the centric array type (dotted arrow) (Figure 4D).

Holotype: A slide of the isolate 180409KCB8B40511, illustrated in Figure 2A–N, was deposited at the Freshwater Bioresources Research Bureau, Nakdonggang National Institute of Biological Resources (slide number FBCC210015D).

Isotype: A slide of the isolate 180409KCB8B40511, illustrated in Figure 2O, was deposited at the Freshwater Bioresources Research Bureau, Nakdonggang National Institute of Biological Resources (slide number FBCC210015D).

Molecular characterization: Nucleotide sequences of the SSU rRNA and *rbcL* genes of strain 180409KCB8B40511 were deposited in GenBank (NCBI; accession numbers MK578710 and MK639354, respectively).

Locality: 37°31'58.90" N, 128°00'42.00" E; Gye Stream, Hoengseong, Korea. Minzi Miao collected the specimen on 4 April 2018.

Etymology: The epithet *ovale* refers to the diatoms' ovate outline.

Habitat: This species is an epilithon diatom that lives in flowing freshwater. The environmental variables of this species' habitat are shown in Table 1.

3.1.2. *Achnantheidium cavitatum* M. Miao & B.-H. Kim, sp. nov.

Figure 5 (LM), Figure 6, and Figure 7 (SEM) here.

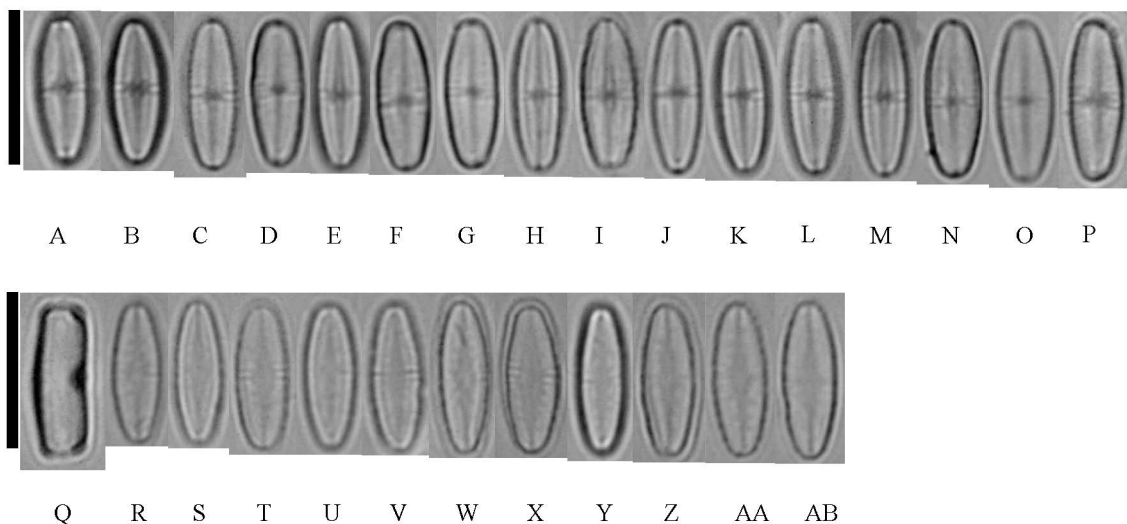


Figure 5. LM of *Achnantheidium cavitatum* sp. nov. taken from the holotype population (180419HG03C4C30524). Scale bar = 10 μ m. (A–P) Raphe view of cell valve. (Q) Girdle view of *A. cavitatum*. (R–AB) Rapheless view of cell valve.

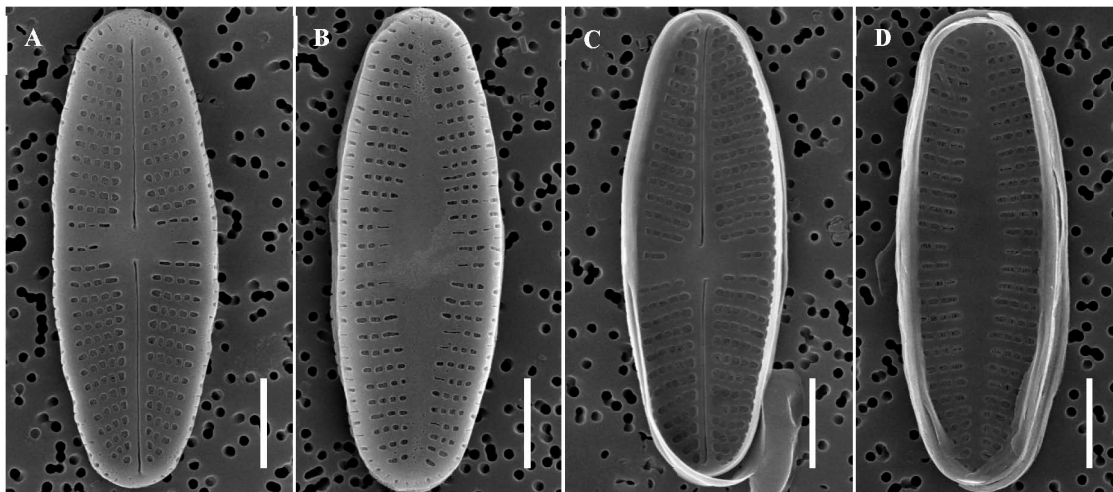


Figure 6. SEM of *Achnanthisdium cavitatum* sp. nov. taken from the holotype population (180419HG03C4C30524). Scale bar = 2 µm. (A) External view of raphe valve with straight terminal raphe fissures. (B) External view of rapheless valve with a broadly lanceolate axial central area. (C) Internal view of raphe valve. (D) Internal view of rapheless valve.

Description: Cells are linear-elliptical with slightly drawn-out ends, 8.8–13.0 µm long, and 3.0–3.5 µm wide. Striae density on the raphe valve is 25–28 in 10 µm in the center and 30–35 in 10 µm at the apices. Striae are radiate at the apices and weakly radiate in the central area. The raphe valve has a linear axial area that becomes wider in the central area. The raphe end is straight at the apices and teardrop-like in the central area. Raphe terminal fissures are absent. Most areolae are round, but some are elongate and slit-like in the central area (Figure 6A,B). Slit-like areolae are more numerous on the rapheless valve than on the raphe valve (Figure 6A,B). Striae are more numerous on the primary side of the raphe and rapheless valves than on the secondary side (Figure 6A,B). On the internal side of the raphe valve, the central raphe endings gently curve in opposite directions (Figure 6C). The central area of rapheless valves is broadly lanceolate to linear and narrow (Figure 6D).

The raphe valves are concave, and the rapheless valves are convex (Figure 7A,B). The axial area is below the valve plane in the rapheless valves (Figure 7B). Areolae on the valve mantle are elongated to slit-like on both raphe and rapheless valves (Figure 7A,B). Internally, there are two types of hymenes, including the valve mantle, in the raphe and rapheless valves (Figure 7C,D, solid arrow). The external valve of the cell can be seen through the broken hymen, which has slit-like openings. Areolae with slit-like openings are loculate (Figure 7D, solid arrow). On the other side, externally, two shapes of areolae can be seen in the raphe and rapheless valves: slit-like (arrow S) to elongate or round (arrow E) (Figure 7E,F). There are two types of areola occlusions: (1) round or elongate-round opening, with hymenes between the external and internal valves; and (2) slit-like opening on the external valve, covered by hymenes on the internal valve plate, different from the round or elongate areolae.

Holotype: A slide of the isolate 180419HG03C4C30524, illustrated in Figure 5A,C–AB, was deposited at the Freshwater Bioresources Culture Research Bureau, Nakdonggang National Institute of Biological Resources (slide number FBCC210016D).

Isotype: A slide of the isolate 180419HG03C4C30524, illustrated in Figure 5B, was deposited at the Freshwater Bioresources Culture Research Bureau, Nakdonggang National Institute of Biological Resources (slide number FBCC210016D).

Molecular characterization: Nucleotide sequences of the SSU rRNA and *rbcl* genes of strain 180419HG03C4C30524 were deposited in GenBank (NCBI; accession numbers MK578711 and MK639355, respectively).

Locality: 38°4′28″ N, 127°24′52″ E; Yeongpyeong Stream, Pocheon, Korea. Minzi Miao collected the specimens on 13 April 2018.

Etymology: The epithet *cavitatum* refers to the specimens' broad axial central area on the rapheless valve.

Habitat: This species is an epilithon diatom and lives in flowing freshwater. The environmental variables of its habitat are shown in Table 1.

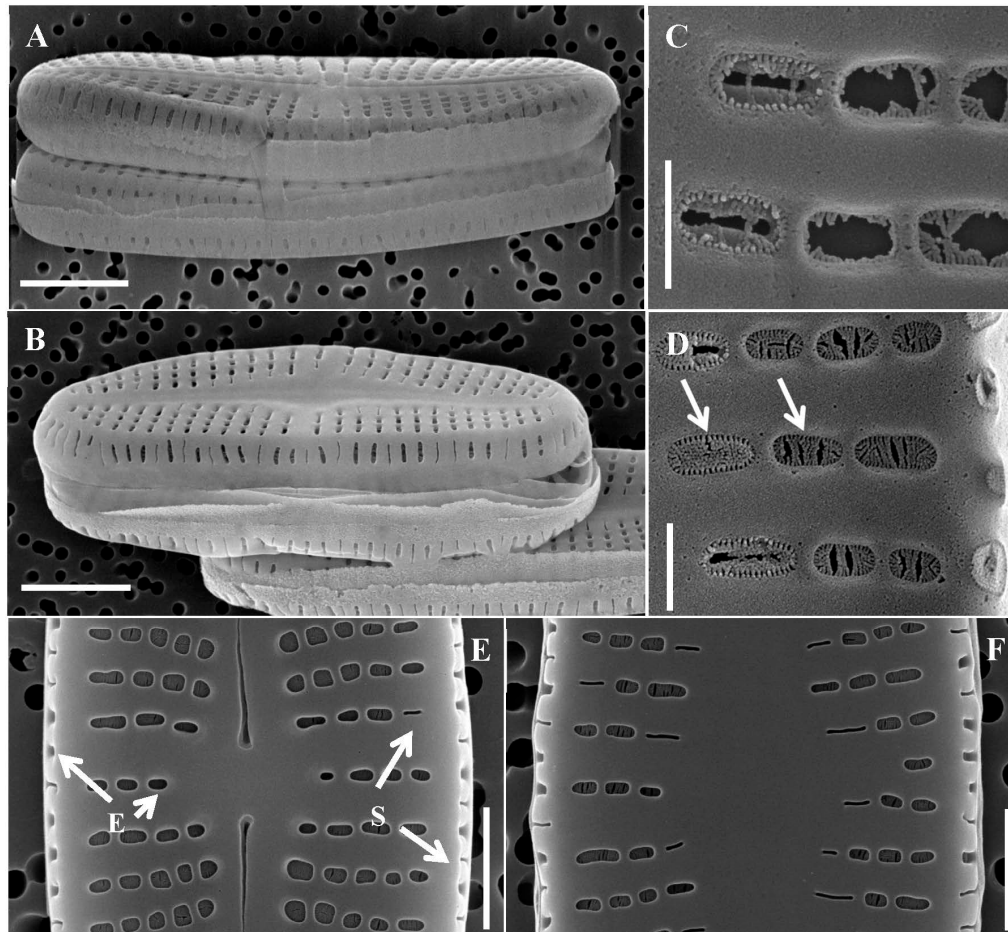


Figure 7. SEM of *Achmanthidium cavitatum* sp. nov. taken from the holotype population (180419HG03C4C30524). (A) Concave raphe valve. Scale bar = 2 μ m. (B) Convex rapheless valve with V shallow axial area. Scale bar = 2 μ m. (C) Internal view on broken hymenes of rapheless valve. The external valve of the cell can be seen through the broken hymen, which has slit liked openings. The areolae with slit-like openings are loculate areolae. Scale bar = 0.3 μ m. (D) Different areolae occlusion on the internal view of rapheless valve and margin area of it (arrows). Scale bar = 0.3 μ m. (E) Teardrop-shaped central raphe endings. Different shapes of areolae on the external view of the raphe valve and margin area. Elongated or rounded shape of areolae on valve plate and side (arrow E). Slit-like areolae on valve plate and sides (arrow S). Scale bar = 1 μ m. (F) Different shapes of areolae on the external view of the rapheless valve and margin area. Scale bar = 1 μ m.

3.2. Molecular Phylogeny

The phylogenetic positions of *Achmanthidium ovale* sp. nov. (HYU-D036) and *Achmanthidium cavitatum* sp. nov. (HYU-D037) were inferred using SSU rRNA and *rbcL* gene sequences (Figures 2G and 8). ML and Bayesian analyses generated four similar trees that differed in only a few topological features. The results of the SSU-generated phylogenetic trees show that sequences of *Achmanthidium* species formed a monophyletic group with high statistical support (100% ML bootstrap support and 1.00 Bayesian posterior probability [PP]) (Figure 8). The phylogenetic positions of *A. ovale* (HYU-D036) and *A. cavitatum* (HYU-D037) were clearly different from those of other *Achmanthidium* species. The similarity scores based on the SSU rRNA data are shown in Table 4. The highest similarity score and lowest *p*-distance of *A. ovale*

were found in the comparisons to *A. reimeri* (Arei2) (0.988) and *A. anastasiae* (Ros1) (0.006), respectively. The highest similarity score and lowest *p*-distance of *A. cavitatum* were found in the comparisons to *A. catenatum* (TCC849) (similarity score = 0.990; *p*-distance = 0.004).

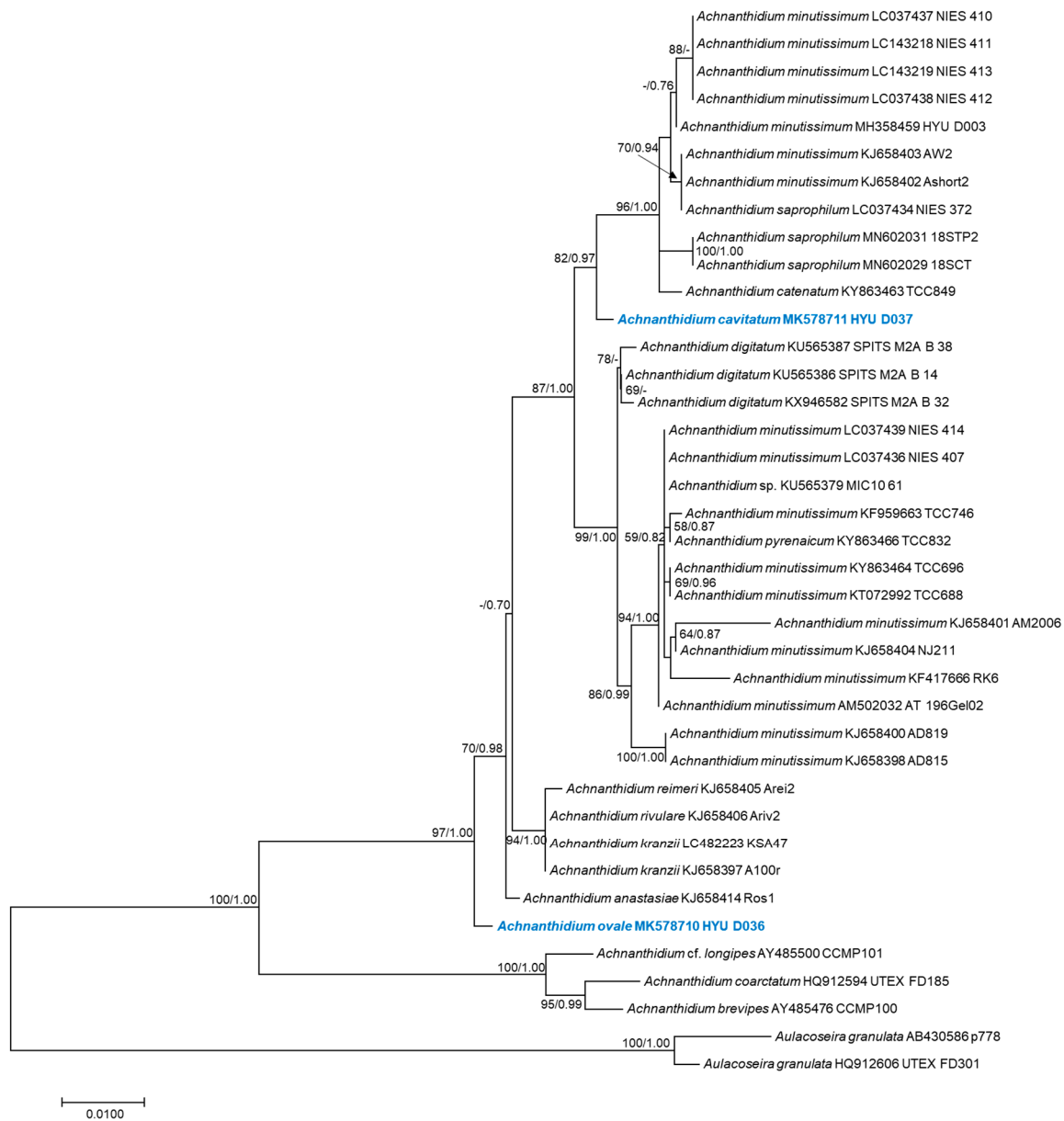


Figure 8. Maximum likelihood phylogenetic tree based on the SSU rRNA gene dataset showing the phylogenetic positions of *Achnanthydium ovale* sp. nov. (HYU-D036) and *A. cavitatum* sp. nov. (HYU-D037). Sequences from *Aulacoseira granulata* were used as the outgroup. The numbers on each node are the bootstrap value (%) and the Bayesian posterior probability (PP). Only bootstrap values above 50 and PP above 0.7 are shown. The GenBank accession and strain numbers follow the taxon names. Scale bar = 0.01 nucleotide substitutions per site.

Table 4. Similarity scores and genetic distances (SSU) of *Achnanthidium* species based on 540 bp of nuclear-encoded SSU rRNA gene sequences. GenBank accession and strain numbers follow the taxon names.

Sequence Name	<i>Achnanthidium ovale</i> MK578710 HYU-D036		<i>Achnanthidium cavitatum</i> MK578711 HYU-D037	
	Similarity	<i>p</i> -Distance	Similarity	<i>p</i> -Distance
<i>Achnanthidium ovale</i> MK578710 HYU-D036	-	-	0.977	0.012
<i>Achnanthidium cavitatum</i> MK578711 HYU-D037	0.977	0.012	-	-
<i>Achnanthidium brevipes</i> AY485476 CCMP100	0.921	0.044	0.913	0.046
<i>Achnanthidium catenatum</i> KY863463 TCC849	0.971	0.016	0.99	0.004
<i>Achnanthidium</i> cf. <i>longipes</i> AY485500 CCMP101	0.912	0.050	0.904	0.052
<i>Achnanthidium coarctatum</i> HQ912594 UTEX FD185	0.915	0.050	0.908	0.052
<i>Achnanthidium digitatum</i> KU565386 SPITS-M2A+B-14	0.969	0.014	0.979	0.014
<i>Achnanthidium digitatum</i> KU565387 SPITS-M2A+B-38	0.967	0.014	0.977	0.014
<i>Achnanthidium digitatum</i> KX946582 SPITS-M2A+B-32	0.969	0.014	0.979	0.014
<i>Achnanthidium kranzii</i> KJ658397 A100r	0.986	0.008	0.979	0.010
<i>Achnanthidium kranzii</i> LC482223 KSA47	0.986	0.008	0.979	0.010
<i>Achnanthidium minutissimum</i> AM502032 AT-196Gel02	0.967	0.018	0.975	0.018
<i>Achnanthidium minutissimum</i> KF417666 RK6	0.935	0.030	0.933	0.030
<i>Achnanthidium minutissimum</i> KF959663 TCC746	0.967	0.018	0.975	0.018
<i>Achnanthidium minutissimum</i> KJ658398 AD815	0.963	0.020	0.977	0.018
<i>Achnanthidium minutissimum</i> KJ658400 AD819	0.963	0.020	0.977	0.018
<i>Achnanthidium minutissimum</i> KJ658401 AM2006	0.965	0.018	0.973	0.018
<i>Achnanthidium minutissimum</i> KJ658402 Ashort2	0.971	0.016	0.986	0.008
<i>Achnanthidium minutissimum</i> KJ658403 AW2	0.971	0.016	0.986	0.008
<i>Achnanthidium minutissimum</i> KJ658404 NJ211	0.963	0.018	0.971	0.018
<i>Achnanthidium minutissimum</i> KT072992 TCC688	0.967	0.018	0.975	0.018
<i>Achnanthidium minutissimum</i> KY863464 TCC696	0.967	0.018	0.975	0.018
<i>Achnanthidium minutissimum</i> LC037436 NIES-407	0.967	0.018	0.975	0.018
<i>Achnanthidium minutissimum</i> LC037437 NIES-410	0.973	0.014	0.98	0.010
<i>Achnanthidium minutissimum</i> LC037438 NIES-412	0.973	0.014	0.98	0.010
<i>Achnanthidium minutissimum</i> LC037439 NIES-414	0.967	0.018	0.975	0.018
<i>Achnanthidium minutissimum</i> LC143218 NIES-411	0.973	0.014	0.98	0.010
<i>Achnanthidium minutissimum</i> LC143219 NIES-413	0.973	0.014	0.98	0.010
<i>Achnanthidium minutissimum</i> MH358459 HYU-D003	0.971	0.016	0.986	0.008
<i>Achnanthidium pyrenaicum</i> KY863466 TCC832	0.967	0.018	0.975	0.018
<i>Achnanthidium reimeri</i> KJ658405 Arei2	0.988	0.006	0.977	0.012
<i>Achnanthidium rivulare</i> KJ658406 Ariv2	0.986	0.008	0.979	0.010
<i>Achnanthidium saprophilum</i> LC037434 NIES-372	0.971	0.016	0.986	0.008
<i>Achnanthidium saprophilum</i> MN602029 18SCT	0.971	0.014	0.979	0.010
<i>Achnanthidium saprophilum</i> MN602031 18STP2	0.971	0.014	0.979	0.010
<i>Achnanthidium anastasiae</i> KJ658414 Ros1	0.988	0.006	0.975	0.010
<i>Achnanthidium</i> sp. KU565379 MIC10 61	0.967	0.018	0.975	0.018

The *rbcL*-generated phylogenetic tree also shows that the position of *A. ovale* (HYU-D036) is distinct from those of other *Achnanthidium* species (Figure 9). *A. cavitatum* (HYU-D037) and *A. straubianum* (TCC831) form a single cluster with strong support (93% ML bootstrap and 1.00 Bayesian PP). The similarity scores based on *rbcL* gene sequences are shown in Table 5. *Achnanthidium ovale* had the highest similarity score (0.956) and lowest genetic distance (0.045) compared with *A. anastasiae* (Ros1), and *A. cavitatum* had the highest similarity score (0.971) and lowest genetic distance (0.028) compared with *A. straubianum* (TCC831).

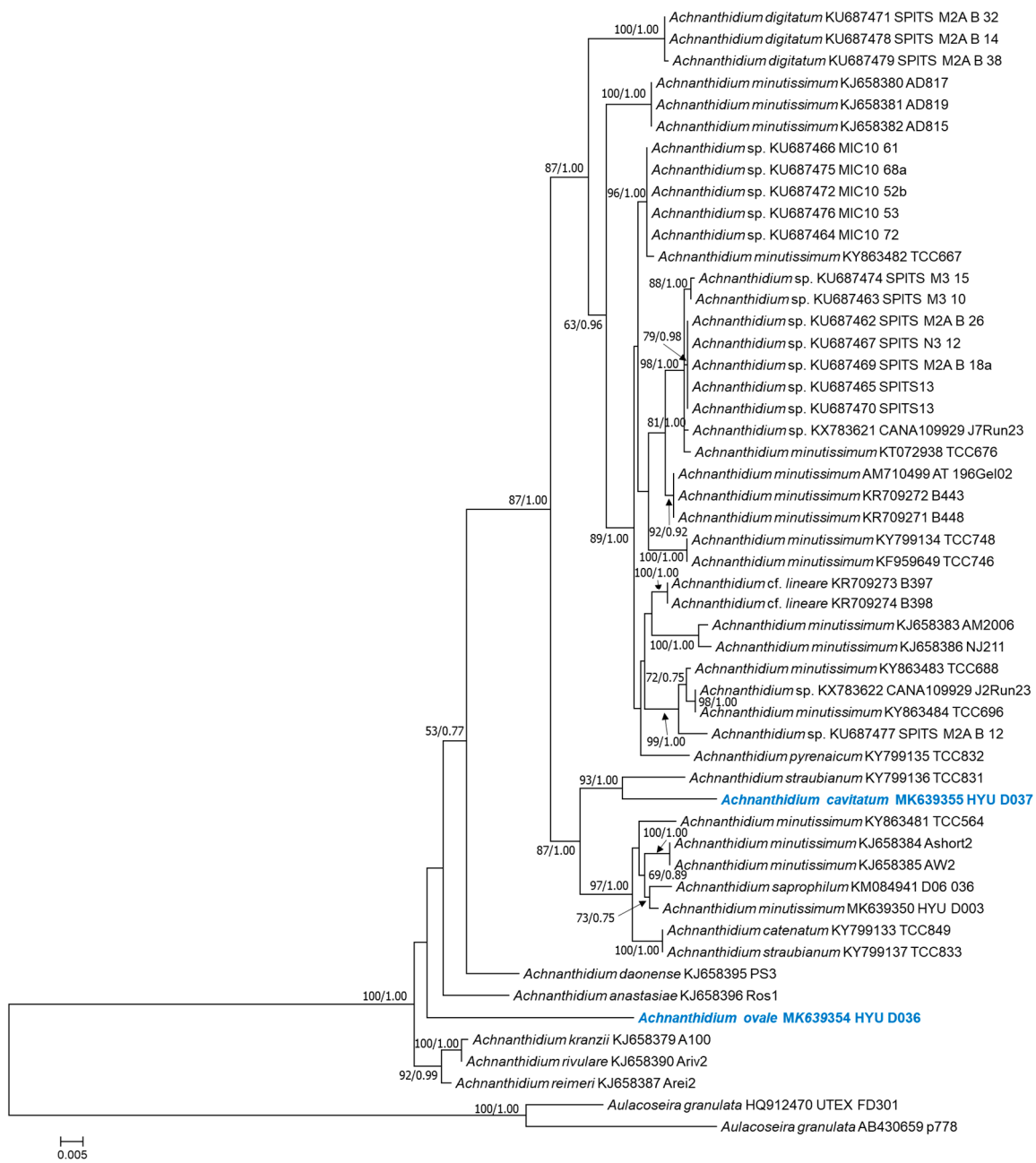


Figure 9. Maximum likelihood phylogenetic tree based on the *rbcL* gene dataset showing the phylogenetic positions of *Achnanthydium ovale* sp. nov. (HYU–D036) and *A. cavitatum* sp. nov. (HYU–D037). Sequences from *Aulacoseira granulata* were used as the outgroup. The numbers on each node are the bootstrap value (%) and the Bayesian posterior probability (PP). Only bootstrap values above 50 and PP above 0.7 are shown. The GenBank accession and strain numbers follow the taxon names. Scale bar = 0.005 nucleotide substitutions per site.

Table 5. Similarity scores and genetic distances of *Achnanthidium* species sequences based on 594 bp of chloroplast-encoded *rbcl* gene sequences. GenBank accession and strain numbers follow the taxon names.

Sequence Name	<i>Achnanthidium ovale</i> MK578710 HYU-D036		<i>Achnanthidium cavitatum</i> MK578711 HYU-D037	
	Similarity	<i>p</i> -Distance	Similarity	<i>p</i> -Distance
<i>Achnanthidium ovale</i> MK639354 HYU-D036	-	-	0.924	0.075
<i>Achnanthidium cavitatum</i> MK639355 HYU-D037	0.924	0.075	-	-
<i>Achnanthidium anastasiae</i> KJ658396 Ros1	0.956	0.045	0.946	0.052
<i>Achnanthidium catenatum</i> KY799133 TCC849	0.925	0.066	0.961	0.033
<i>Achnanthidium cf. lineare</i> KR709273 B397	0.930	0.068	0.957	0.043
<i>Achnanthidium cf. lineare</i> KR709274 B398	0.930	0.068	0.957	0.043
<i>Achnanthidium daonense</i> KJ658395 PS3	0.937	0.064	0.941	0.057
<i>Achnanthidium digitatum</i> KU687471 SPITS-M2A+B-32	0.936	0.063	0.954	0.047
<i>Achnanthidium digitatum</i> KU687478 SPITS-M2A+B-14	0.936	0.063	0.954	0.047
<i>Achnanthidium digitatum</i> KU687479 SPITS-M2A+B-38	0.934	0.064	0.952	0.049
<i>Achnanthidium kranzii</i> KJ658379 A100	0.944	0.057	0.929	0.070
<i>Achnanthidium minutissimum</i> AM710499 AT-196Gel02	0.936	0.063	0.959	0.042
<i>Achnanthidium minutissimum</i> KF959649 TCC746	0.934	0.064	0.954	0.047
<i>Achnanthidium minutissimum</i> KJ658380 AD817	0.936	0.063	0.954	0.047
<i>Achnanthidium minutissimum</i> KJ658381 AD819	0.936	0.063	0.954	0.047
<i>Achnanthidium minutissimum</i> KJ658382 AD815	0.936	0.063	0.954	0.047
<i>Achnanthidium minutissimum</i> KJ658383 AM2006	0.934	0.064	0.954	0.047
<i>Achnanthidium minutissimum</i> KJ658384 Ashort2	0.929	0.070	0.966	0.035
<i>Achnanthidium minutissimum</i> KJ658385 AW2	0.929	0.070	0.966	0.035
<i>Achnanthidium minutissimum</i> KJ658386 NJ211	0.937	0.061	0.956	0.045
<i>Achnanthidium minutissimum</i> KR709271 B448	0.936	0.063	0.959	0.042
<i>Achnanthidium minutissimum</i> KR709272 B443	0.936	0.063	0.959	0.042
<i>Achnanthidium minutissimum</i> KT072938 TCC676	0.937	0.061	0.957	0.043
<i>Achnanthidium minutissimum</i> KY799134 TCC748	0.932	0.064	0.951	0.047
<i>Achnanthidium minutissimum</i> KY863481 TCC564	0.927	0.070	0.968	0.031
<i>Achnanthidium minutissimum</i> KY863482 TCC667	0.936	0.063	0.962	0.038
<i>Achnanthidium minutissimum</i> KY863483 TCC688	0.934	0.064	0.959	0.042
<i>Achnanthidium minutissimum</i> KY863484 TCC696	0.930	0.068	0.956	0.045
<i>Achnanthidium minutissimum</i> MK639350 HYU-D003	0.930	0.068	0.966	0.035
<i>Achnanthidium pyrenaicum</i> KY799135 TCC832	0.919	0.070	0.942	0.049
<i>Achnanthidium reimeri</i> KJ658387 Arei2	0.952	0.049	0.932	0.066
<i>Achnanthidium rivulare</i> KJ658390 Ariv2	0.944	0.057	0.929	0.070
<i>Achnanthidium saprophilum</i> KM084941 D06-036	0.927	0.071	0.962	0.038
<i>Achnanthidium straubianum</i> KY799136 TCC831	0.925	0.073	0.971	0.028
<i>Achnanthidium straubianum</i> KY799137 TCC833	0.922	0.066	0.957	0.033
<i>Achnanthidium</i> sp. KU687462 SPITS-M2A+B-26	0.934	0.064	0.957	0.043
<i>Achnanthidium</i> sp. KU687463 SPITS-M3-10	0.932	0.064	0.959	0.040
<i>Achnanthidium</i> sp. KU687464 MIC10-72	0.936	0.063	0.962	0.038
<i>Achnanthidium</i> sp. KU687465 SPITS13	0.934	0.064	0.957	0.043
<i>Achnanthidium</i> sp. KU687466 MIC10-61	0.936	0.063	0.962	0.038
<i>Achnanthidium</i> sp. KU687467 SPITS-N3-12	0.934	0.064	0.957	0.043
<i>Achnanthidium</i> sp. KU687469 SPITS-M2A+B-18a	0.934	0.064	0.957	0.043
<i>Achnanthidium</i> sp. KU687470 SPITS13	0.934	0.064	0.957	0.043
<i>Achnanthidium</i> sp. KU687472 MIC10-52b	0.936	0.063	0.962	0.038
<i>Achnanthidium</i> sp. KU687474 SPITS-M3-15	0.932	0.064	0.959	0.040
<i>Achnanthidium</i> sp. KU687475 MIC10-68a	0.936	0.063	0.962	0.038
<i>Achnanthidium</i> sp. KU687476 MIC10-53	0.936	0.063	0.962	0.038
<i>Achnanthidium</i> sp. KU687477 SPITS-M2A+B-12	0.930	0.068	0.956	0.045
<i>Achnanthidium</i> sp. KX783621 CANA109929-J7Run23	0.936	0.063	0.959	0.042
<i>Achnanthidium</i> sp. KX783622 CANA109929-J2Run23	0.930	0.068	0.956	0.045

4. Discussion

4.1. *Achnantheidium ovale* as a New Species

Achnantheidium ovale sp. nov. has terminal raphe endings that turn to the same side. This characteristic is typical of species belonging to the *A. pyrenaicum* complex. Table 6 shows a detailed comparison between *A. ovale* and similar species from the *A. pyrenaicum* complex taxa: *A. rivulare* Potapova & Ponader [10], *A. pyrenaicum* (Hustedt) Kobayasi (Karthick et al. [13]), and *A. convergens* Kobayasi [45]. Although the smaller *A. rivulare* is similar to *A. ovale* in valve outline, these species differ in (1) areola openings, (2) striation pattern on the raphe valve, and (3) internal raphe endings. The areola openings in *A. ovale* are mostly elongated or sometimes small and rounded, unlike the areolae in *A. rivulare*, which are mostly rounded. The striae on the apical area of the raphe valve in *A. ovale* are radiate, unlike the convergent striae of *A. rivulare*. Internally, *A. ovale* has deflected raphe central endings, whereas *A. rivulare* has hooked raphe central endings. In *A. rivulare*, the number of mantle areolae at the valve ends that do not correspond to the areolae on the valve face varies between 1 and 4 but is usually 2 or 3 ([10]; Figure 5E–K,M,S); however, in *A. ovale*, the number of areolae that do not have corresponding areolae on the valve face is as high as 5 (Figure 3A). According to Kobayasi [5], the number of freestanding areolae is a species-specific characteristic in *Achnantheidium*. Potapova & Ponader [10] considered that the number of areolae varied not only among species, but also within a single valve. *Achnantheidium ovale* differs from *A. pyrenaicum* in outline, as the latter has slightly drawn-out ends. Moreover, the outline and striation pattern of *A. ovale* differ from those of *A. convergens*. In both SSU rRNA and *rbcL* phylogenetic trees, *A. ovale* has a unique phylogenetic position, as appropriate to establish a new species. In addition, it is slightly related to *A. daonense* and *A. anastasiae* in the *A. minutissimum* complex, with less support.

4.2. *Achnantheidium cavitatum* as a New Species

Achnantheidium cavitatum has straight terminal raphe endings, which is characteristic of members of the *A. minutissimum* complex. Table 7 shows a detailed comparison between *A. cavitatum* and similar species from the *A. minutissimum* complex: *A. minutissimum* [6], *A. saprophilum* Round and Bukhtiyarova (Hlubikova et al. [24]), *A. eutrophilum* Lange-Bertalot (Hlubikova et al. [24]), and *A. duriense* Novais & Ector (Novais et al. [16]).

Achnantheidium cavitatum has two conspicuous characteristics that are typically observed in species from the *A. minutissimum* complex: (a) axial central area broadly lanceolate to linear and narrow, which can be observed under LM (Figure 5R–AB), and (b) slit-like areolae, mostly near the axial central area, which can be observed using SEM (Figures 6B and 7B,F). On the other hand, *A. cavitatum* differs from *A. minutissimum* in outline and *A. saprophilum* in outline and number of areolae per stria. Moreover, *A. cavitatum* differs from *A. eutrophilum* in outline and central area of the raphe valve and from *A. duriense* in outline and areola arrangement on internal view [16].

The SSU rRNA and *rbcL* gene phylogenetic trees indicate that *A. cavitatum* is part of the clade containing *Achnantheidium* strains (Figures 2G and 8). Therefore, based on its morphological characteristics and molecular data, it is correct to classify *A. cavitatum* in the genus *Achnantheidium*. The axial central area of *A. cavitatum* differs from those of other *Achnantheidium* species. In addition, the molecular data show that *A. cavitatum* has low genetic distance and similarity scores compared to sequences from the NCBI database (Table 4; Table 5). Therefore, we propose *A. cavitatum* as a new *Achnantheidium* species based on morphological and molecular analyses.

Table 6. Morphological comparison between *Achnantheidium ovale* sp. nov. and similar species.

	<i>A. ovale</i> M. Miao & B.-H. Kim sp. nov.	<i>A. rivulare</i> Potapova & Ponader	<i>A. pyrenaicum</i> (Hustedt) Kobayasi	<i>A. convergens</i> Kobayasi
length (µm)	6.3–7.7	5.4–21.3	10.0–16.0	10.0–25.0
width (µm)	3.8–4.1	2.6–4.4	2.5–4.0	4–4.5
valve outline	elliptical	linear-elliptical	linear-lanceolate with slightly drawn-out ends	linear-lanceolate
external areolae	elongate and dot-like	small, round, or slightly elongated	elongate or circular (RV)	constricted in various degrees.
internal areolae	hymenes partially joined	elliptical internal openings occluded by hymenes	hymenes not joined	hymenes partially joined, linking bars between interstriae partly interrupted
areolae in valve mantle	slit-like	slit-like	elongate	elongate
raphe valve				
density of striae (in 10 µm)	30–35 (up to 55 near apices)	19–25 (up to 55 near apices)	center: 20–25 apices: 34–40	center: 18, apices: 36–40
striation pattern	parallel but slightly radiate at apices	parallel but convergent or parallel near apices	parallel or slightly radiate in the central area and slightly convergent at apices	densely convergent striae near the valve ends
external raphe endings	laterally expanded	teardrop-shaped	teardrop-shaped	laterally expanded
internal raphe endings	deflected in opposite directions	short, hook-shaped	slightly curved to opposite sides	deflected in opposite directions
rapheless valve				
density of striae (in 10 µm)	30–33 (up to 50 near apices)	19–28 (up to 43 near apices)	center: 20–28 apices: 32–38	
striation pattern	parallel but slightly radiate near apices	parallel but slightly radiate near apices	parallel or slightly radiate in the central area and slightly convergent at apices	slightly radiate at the ends
source	this study	[10]	[13]	[45]

Table 7. Morphological comparison between *Achnantheidium cavitatum* sp. nov. and similar species.

	<i>A. cavitatum</i> M. Miao & B.-H. Kim sp. Nov.	<i>A. minutissimum</i> (Kützing) Czarnecki	<i>A. saprophilum</i> (Kobayashi & Mayama) Round & Bukhtiyarova	<i>A. eutrophilum</i> (Lange-Bertalot) Lange-Bertalot	<i>A. duriense</i> Novais & Ector
length (µm)	8.8–10.3	9.0–14.5	9.5–14.5	7.5–16.0	5.0–9.7
width (µm)	3.0–3.5	2.5–3.177	3.0–3.6	3.2–4.8	2.0–2.7
valve outline	rhombic with slightly drawn-out ends	linear-elliptic to linear-lanceolate	broadly linear	narrowly rhombic	elliptic to linear-elliptic
striation pattern	radiate at apices and weakly radiate in central area	radiate, denser toward the apices	radiate at apices and weakly radiate in central area	radiate at apices and weakly radiate in central area	almost parallel near the center; slightly radiate elsewhere
areolae in the valve mantle	slit-like or elongate	slit-like	slit-like	elongate or slit-like	elongate or slit-like
raphe valve					
density of striae (in 10 µm)	30–32	30–35	28–31	25–30	35
areola openings	most areolae are rounded or elongate elliptic; some are slit-like in the central area	small and rounded; slit-like near the margin	rounded; slit-like near the margin	rounded to elongated areolae	quadrangular or rounded
central area	linear, becoming a little wider in the central area	small and lanceolate to rectangular	linear, becoming a little wider in the central area	small rhombic, almost absent	narrow linear axial area slightly expanded towards the center
rapheless valve					
density of striae (in 10 µm)	28–40	32–35	28–31	25–30	35
areola openings	most areolae are rounded or elongated elliptic, but some are slit-like; slit-like areolae are mostly in the axial central area and more than RV	small and rounded; slit-like near the margin	rounded; slit-like near the margin	rounded to elongated	quadrangular or rounded; sometimes slit-like near the margin
central area	broadly lanceolate to linear and narrow	narrowly lanceolate	broadly lanceolate to linear and narrow	narrowly rhombic to lanceolate, almost absent	narrow, linear axial area slightly widening toward the central area
Source	this study	[6]	[24]	[24]	[16]

4.3. Areolae Occlusions and Openings

Loculate areolae are markedly constricted at one surface and occluded [19] by a velum (cribrum, rota, vola) or a hymen at the other. Yana & Mayama [23] described *A. pseudoconspicuum* var. *yomensis* to have loculate type areolae and incomplete vimines through lost hymenes. In the present study, we found a similar arrangement in *A. ovale*: the ultrastructure of the loculate areolae can be seen from the broken valve. Moreover, most *A. ovale* vimines are incomplete, and the hymens have different thicknesses from the margin area to the central area. However, *A. cavitatum* also has a different ultrastructure of the valve on the internal view. In the external view, the areola openings are slit-like or round and elongate on both the valve face and mantle (Figure 7A,B). On the internal view, slit-like and elongate areola openings can be seen through broken hymenes, and vimines are complete between areolae. Around the rapheless valve, the slit-like areola openings occluded by hymenes differ from the hymenes occluded by elongate areolae openings, depending on the depth of the valve (Figure 7D). Thomas [46] recognized the areola type of *A. minutissimum* as poroid. However, using SEM, we observed that the areolae of *Achnanthidium* are loculated and internally covered by hymenes.

4.4. Ecological Characteristics of Two *Achnanthidium* Species

Achnanthidium ovale sp. nov. and *A. cavitatum* sp. nov. were recorded in the Gye Stream and the Yeongpyeong Stream (Korea), respectively. The summary of environmental data is shown in Table 1. Previous studies on *Achnanthidium* stated that species of this genus live in alkaline to acidic environments [14]; this is supported by the results of the present study. *Achnanthidium ovale* and *A. minutissimum* were collected from an alkaline environment, whereas *A. cavitatum* was collected from an acidic environment. The water velocity in the location of the two species was 0–80 cm/s (Table 1). Dissolved oxygen (5.93–9.86 mg/L), water temperature (4.10–11.71 °C), conductivity (57–148 µS/Cm), and turbidity (0.0–5.4 NTU) in the two locations differed widely. Studies have shown that water-quality assessment methods can be based on genus-level identifications because species within a genus can live in different ecological conditions [15,47–49]. The two species in our study, although they are from the same genus, live in different pH, dissolved oxygen, water temperature, velocity, conductivity, and turbidity conditions; therefore, our results support previous conclusions about the genus *Achnanthidium*.

Achnanthidium ovale was collected from a stone in Gye Stream, which has a fast flow and low conductivity and turbidity. Land use and cover conditions within a 1 km radius of this area are forest (50%) and agriculture (50%) [50]. The dominant species here is *A. minutissimum* (77.31%), a widespread species found in low abundance in polluted rivers [15].

Achnanthidium cavitatum was collected from a stone in the Yeongpyeong Stream, which is a slightly acidic environment with low conductivity and turbidity. Land use and cover conditions of this area are forest (80%) and urban (20%) [50]. The stream is fast-flowing and has a stony substratum. The dominant species in this area is *Hannaea arcus* var. *recta* Idei (41.33%), which is a saproxenous species [51]. The subdominant species is *Achnanthidium minutissimum* (22.45%).

Author Contributions: M.M. and B.-H.K. conceived the research; M.M., H.-K.K., H.L., E.A.-H., and B.-H.K. performed fieldwork; M.M. and Z.L. analyzed the data; M.M., Z.L., and B.-H.K. wrote and edited the manuscript. All authors have read and agreed to the published version of the manuscript.

Funding: This study was partly supported by Hyperspectral Remote Sensing of Algal Distribution of Inherent Optical Properties (NIER-RP2018) and the KRIBB Research Initiative Program.

Acknowledgments: The authors thank the two anonymous referees for their valuable and constructive comments.

Conflicts of Interest: The authors report no potential conflict of interest.

References

1. Patrick, R.; Reimer, C.W. *The Diatoms of the United States Exclusive of Alaska and Hawaii*; Academy of the Natural Sciences: Philadelphia, PA, USA, 1966; p. 688.
2. Round, F.E.; Crawford, R.M.; Mann, D.G. *Diatoms: Biology and Morphology of the Genera*; Cambridge University Press: Cambridge, UK, 1990.
3. Czarnecki, D.B. The freshwater diatoms culture collection at Loras College, Dubuque, Iowa. *Mem. Calif. Acad. Sci.* **1994**, *17*, 155–174.
4. Round, F.E.; Bukhtiyarova, L. Four new genera based on *Achnanthes* (*Achnanthidium*) together with a re-definition of *Achnanthidium*. *Diatom Res.* **1996**, *11*, 345–361. [[CrossRef](#)]
5. Kobayashi, H. Comparative Studies among Four Linear-Lanceolate *Achnanthidium* Species (Bacillariophyceae) with curved terminal raphe endings. *Nova Hedwigia* **1997**, *65*, 147–163. [[CrossRef](#)]
6. Potapova, M.; Hamilton, P.B. Morphological and ecological variation within the *Achnanthidium minutissimum* (Bacillariophyceae) species complex. *J. Phycol.* **2007**, *43*, 561–575. [[CrossRef](#)]
7. Yu, P.; Kocielek, J.P.; You, Q.M.; Wang, Q.X. *Achnanthidium longissimum* sp. nov. (Bacillariophyta), a new diatom species from Jiuzhai Valley, Southwestern China. *Diatom Res.* **2018**, *33*, 339–348. [[CrossRef](#)]
8. Witkowski, A.; Kulikovskiy, M.; Riaux-Gobin, C. *Achnanthidium sieminskae*, a new diatom species from the Kerguelen Archipelago (Austral Islands). In *Current Advances in Algal Taxonomy and Its Applications: Phylogenetic, Ecological and Applied Perspective*; Wołowski, K., Kaczmarska, I., Ehrman, J.M., Wojtal, A.Z., Eds.; Polish Academy of Sciences: Kraków, Poland, 2012; pp. 61–68.
9. Pérès, F.; Le Cohu, R.; Delmont, D. *Achnanthidium barbei* sp. nov. and *Achnanthidium costei* sp. nov., two new diatom species from French rivers. *Diatom Res.* **2014**, *29*, 387–397. [[CrossRef](#)]
10. Potapova, M.G.; Ponader, K.C. Two common North American diatoms, *Achnanthidium rivulare* sp. nov. and *A. deflexum* (Reimer) Kingston: Morphology, ecology and comparison with related species. *Diatom Res.* **2004**, *19*, 33–57. [[CrossRef](#)]
11. Wojtal, A.Z.; Ector, L.; Van de Vijver, B.; Morales, E.A.; Blanco, S.; Piątek, J.; Smieja, A. The *Achnanthidium minutissimum* complex (Bacillariophyceae) in southern Poland. *Algol. Stud.* **2011**, *136*, 211–238. [[CrossRef](#)]
12. Pérès, F.; Barthès, A.; Ponton, E.; Coste, M.; Ten-Hage, L.; Le Cohu, R. *Achnanthidium delmontii* sp. nov., a new species from French rivers. *Fottea* **2012**, *12*, 189–198. [[CrossRef](#)]
13. Karthick, B.; Taylor, J.C.; Hamilton, P.B. Two new species of *Achnanthidium* Kützing (Bacillariophyceae) from Kolli Hills, Eastern Ghats, India. *Fottea* **2017**, *17*, 65–77. [[CrossRef](#)]
14. Martín, G.; Toja, J.; Sala, S.E.; De los Reyes Fernández, M.; Reyes, I.; Casco, M.A. Application of diatom biotic indices in the Guadalquivir River Basin, a Mediterranean basin. Which one is the most appropriated? *Environ. Monit. Assess.* **2010**, *170*, 519–534. [[CrossRef](#)] [[PubMed](#)]
15. Ponader, K.C.; Potapova, M.G. Diatoms from the genus *Achnanthidium* inflowing waters of the Appalachian Mountains (North America): Ecology, distribution and taxonomic notes. *Limnologica* **2007**, *37*, 227–241. [[CrossRef](#)]
16. Novais, M.H.; Juttner, I.; Van de Vijver, B.; Morais, M.M.; Hoffmann, L.; Ector, L. Morphological variability within the *Achnanthidium minutissimum* species complex (Bacillariophyta): Comparison between the type material of *Achnanthes minutissima* and related taxa, and new freshwater *Achnanthidium* species from Portugal. *Phytotaxa* **2015**, *224*, 101–139. [[CrossRef](#)]
17. Cox, E.J. Ontogeny, homology, and terminology—Wall morphogenesis as an aid to character recognition and character state definition for pennate diatom systematics. *J. Phycol.* **2012**, *48*, 1–31. [[CrossRef](#)] [[PubMed](#)]
18. Cox, E.J. Symmetry and valve structure in naviculoid diatoms. *Nova Hedwigia* **1979**, *64*, 193–206.
19. Cox, E.J. Variation in patterns of valve morphogenesis between representatives of six biraphid diatom genera (Bacillariophyceae). *J. Phycol.* **1999**, *35*, 1297–1312. [[CrossRef](#)]
20. Ross, R.; Cox, E.J.; Karayeva, N.I.; Mann, D.G.; Paddock, T.B.B.; Simonsen, R.; Sims, P.A. An amended terminology for the siliceous components of the diatom cell. *Nova Hedwigia* **1979**, *64*, 513–533.
21. Mann, D.G. Sieves and Flaps: Siliceous Minutiae in the Pores of Raphid Diatoms. In *Proceedings of the 6th Symposium on Recent and Fossil Diatoms*; Ross, R., Ed.; O. Koeltz: Koenigstein, Germany, 1981; pp. 279–300.
22. Cox, E.J. Morphogenetic information and the selection of taxonomic characters for raphid diatom systematics. *Plant Ecol. Evol.* **2010**, *143*, 271–277. [[CrossRef](#)]

23. Yana, E.; Mayama, S. Two new taxa of *Achnantheidium* and *Encyonema* (Bacillariophyceae) from the Yom River, Thailand, with special reference to the areolae occlusions implying ontogenetic relationship. *Phycol. Res.* **2015**, *63*, 239–252. [[CrossRef](#)]
24. Hlubikova, D.; Ector, L.; Hoffmann, L. Examination of the type material of some diatom species related to *Achnantheidium minutissimum* (Kütz.) Czarn. (Bacillariophyceae). *Algol. Stud.* **2011**, *136*, 19–43. [[CrossRef](#)]
25. Bruder, K.; Medlin, L.K. Molecular assessment of phylogenetic relationships in selected species/genera in the naviculoid diatoms (Bacillariophyta). I. The genus *Placoneis*. *Nova Hedwigia* **2007**, *85*, 331–352. [[CrossRef](#)]
26. Medlin, L.K.; Kaczmarska, I. Evolution of the diatoms: V. Morphological and cytological support for the major clades and a taxonomic revision. *Phycologia* **2004**, *43*, 245–270. [[CrossRef](#)]
27. Medlin, L.K.; Williams, D.M.; Sims, P.A. The evolution of the diatoms (Bacillariophyta). I. Origin of the group and assessment of the monophyly of its major divisions. *Eur. J. Phycol.* **1993**, *28*, 261–275. [[CrossRef](#)]
28. Medlin, L.K.; Cooper, A.; Hill, C.; Wrieden, S.; Wellbrock, U. Phylogenetic position of the Chromista plastids based on small subunit rRNA coding regions. *Curr. Genet.* **1995**, *28*, 560–565. [[CrossRef](#)] [[PubMed](#)]
29. Medlin, L.K.; Kooistra, W.H.; Gersonde, R.; Wellbrock, U. Evolution of the diatoms (Bacillariophyta). II. Nuclear-encoded small-subunit rRNA sequence comparisons confirm a paraphyletic origin for the centric diatoms. *Mol. Biol. Evol.* **1996**, *13*, 67–75. [[CrossRef](#)]
30. Sorhannus, U. Diatom phylogenetics inferred based on direct optimization of nuclear-encoded SSU rRNA sequences. *Cladistics* **2004**, *20*, 487–497. [[CrossRef](#)]
31. Sato, S.; Mann, D.G.; Matsumoto, S.; Medlin, L.K. *Pseudostriatella* (Bacillariophyta): A description of a new araphid diatom genus based on observations of frustule and auxospore structure and 18S rDNA phylogeny. *Phycologia* **2008**, *47*, 371–391. [[CrossRef](#)]
32. Wang, P.; Park, B.S.; Kim, J.H.; Kim, J.H.; Lee, H.O.; Han, M.S. Phylogenetic position of eight *Amphora sensu lato* (Bacillariophyceae) species and comparative analysis of morphological characteristics. *Algae* **2014**, *29*, 57–73. [[CrossRef](#)]
33. Guo, L.; Sui, Z.; Zhang, S.; Ren, Y.; Liu, Y. Comparison of potential diatom ‘barcode’ genes (the 18S rRNA gene and ITS, COI, rbcL) and their effectiveness in discriminating and determining species taxonomy in the Bacillariophyta. *Int. J. Syst. Evol. Microbiol.* **2015**, *65*, 1369–1380. [[CrossRef](#)] [[PubMed](#)]
34. Mann, D.G.; Simpson, G.E.; Sluiman, H.J.; Möller, M. rbcL gene tree of diatoms: A second large Data-Set for phylogenetic reconstruction. *Phycologia* **2001**, *40*, 1–2.
35. Kulikovskiy, M.S.; Andreeva, S.A.; Gusev, E.S.; Kuznetsova, I.V.; Annenkova, N.V. Molecular phylogeny of monoraphid diatoms and raphe significance in evolution and taxonomy. *Biol. Bull.* **2016**, *43*, 398–407. [[CrossRef](#)]
36. Shi, Y.; Wang, P.; Kim, H.K.; Lee, H.; Han, M.S.; Kim, B.H. *Lemnicola hungarica* (Bacillariophyceae) and the new monoraphid diatom *Lemnicola uniseriata* sp. nov. (Bacillariophyceae) from Korea. *Diatom Res.* **2018**, *33*, 69–87. [[CrossRef](#)]
37. Andersen, R.A. *Algal Culturing Techniques*; Academic Press: San Diego, CA, USA, 2005; p. 578.
38. Beakes, G.W.; Canter, H.M.; Jaworski, G.H.M. Zoospore ultrastructure of *Zygorhizidium affluens* and *Z. planktonicum*, two chytrids parasitizing the diatom *Asterionella formosa*. *Can. J. Bot.* **1988**, *66*, 1054–1067. [[CrossRef](#)]
39. Katano, T.; Lee, J.; Ki, J.S.; Kang, S.H.; Han, M.S. Effects of temperature and salinity on the growth and the optimum nitrogen to phosphorus ratio for the culture of *Diatoma tenue* isolated from a temporary Arctic pond in Svalbard, Norway. *J. Freshw. Ecol.* **2007**, *22*, 629–635. [[CrossRef](#)]
40. Ki, J.S.; Han, M.S. Molecular analysis of complete SSU to LSU rRNA sequence in the harmful dinoflagellate *Alexandrium tamarensense* (Korean isolate, HY970328M). *Ocean Sci. J.* **2005**, *40*, 155–166. [[CrossRef](#)]
41. Thompson, J.D.; Higgins, D.G.; Gibson, T.J. CLUSTAL W: Improving the sensitivity of progressive multiple sequence alignment through sequence weighting, position-specific gap penalties and weight matrix choice. *Nucleic Acids Res.* **1994**, *22*, 4673–4680. [[CrossRef](#)]
42. Kumar, S.; Stecher, G.; Tamura, K. MEGA7: Molecular evolutionary genetics analysis version 7.0 for bigger datasets. *Mol. Biol. Evol.* **2016**, *33*, 1870–1874. [[CrossRef](#)] [[PubMed](#)]
43. Stamatakis, A. RAxML version 8: A tool for phylogenetic analysis and post-analysis of large phylogenies. *Bioinformatics* **2014**, *30*, 1312–1313. [[CrossRef](#)] [[PubMed](#)]

44. Fredrik, R.; Teslenko, M.; Van der Mark, P.; Ayres, D.L.; Darling, A.; Höhna, S.; Larget, B.; Liu, L.; Suchard, M.A.; Huelsenbeck, J.P. MrBayes 3.2: Efficient Bayesian phylogenetic inference and model choice across a large model space. *Syst. Biol.* **2012**, *61*, 539–542.
45. Kobayasi, H.; Nagumo, T.; Mayama, S. Observation on the two rheophilic species of the genus *Achnanthes* (Bacillariophyceae), *A. convergens* H. Kob. And *A. japonica* H. Kob. *Diatom* **1986**, *2*, 83–93.
46. Thomas, E.W. Exploring Species Boundaries in the Diatom Genus *Rhoicosphenia* Using Morphology, Phylogeny, Ecology, and Biogeography. Ph.D. Thesis, Department of Ecology & Evolutionary, University of Colorado, Boulder, Co, USA, 2016.
47. Chessman, B.; Grown, I.; Currey, J.; Plunkett-Cole, N. Predicting diatom communities at the genus level for the rapid biological assessment of rivers. *Freshw. Biol.* **1999**, *41*, 317–331. [[CrossRef](#)]
48. Wu, J.T. A generic index of diatom assemblages as bioindicator of pollution in the Keelung River of Taiwan. *Hydrobiologia* **1999**, *397*, 79–87. [[CrossRef](#)]
49. Hill, B.H.; Herlihy, A.T.; Kaufmann, P.R.; Stevenson, R.J.; McCormick, F.H.; Johnson, C.B. Use of periphyton assemblage data as an index of biotic integrity. *J. N. Am. Bent. Soc.* **2000**, *19*, 50–67. [[CrossRef](#)]
50. NGII (National Geographic Information Institute). Available online: <https://www.ngii.go.kr/> (accessed on 11 June 2020).
51. Kobayasi, H.; Idei, M.; Mayama, S.; Nagumo, T.; Osada, K. *Kobayasi's Atlas of Japanese Diatoms Based on Electron Microscopy*; Uchida Rokakuho: Tokyo, Japan, 2006; p. 531.



© 2020 by the authors. Licensee MDPI, Basel, Switzerland. This article is an open access article distributed under the terms and conditions of the Creative Commons Attribution (CC BY) license (<http://creativecommons.org/licenses/by/4.0/>).